Remaining Useful Lifetime estimation for Electronic Power modules using an analytical degradation model

Mohamad Nazar[1, 2], Ali Ibrahim[1], Zoubir Khatir[1], Nicolas Degrenne[2], Zeina Al Masry[3]

[1]*SATIE Lab., Gustave Eiffel University, Versailles, 78000, France*
Mohamad.Nazar@univ-eiffel.fr
Ali.Ibrahim@univ-eiffel.fr
Zoubir.Khatir@univ-eiffel.fr

[2]*Mitsubishi Electric R&D Center Europe (MERCE), 35708 Rennes, France*
N.Degrenne@fr.merce.mee.com

[3]*FEMTO-ST Institute, Univ. Bourgogne Franche-Comté, CNRS, ENSMM, 25000 Besançon, France*
Zeina.Al.Masry@ens2m.fr

ABSTRACT

Power electronic modules undergo electro-thermal stresses due to power losses that lead to several kinds of degradations, and finally to failure. In order to prevent power electronic module failure, one should assess its state of health in real-time operation. For this purpose, Prognostics and Health Management (PHM) approach could be a promising tool for reliability evaluation for an IGBT device. The Insulated Gate Bipolar Transistor is a three-terminal power semiconductor device used as an electronic switch which combines high efficiency and fast switching. In this paper, an analytical model is proposed that describes the metallization to wire-bond contact resistance. This model computes the crack length and then using online measurement the rate of crack propagation is computed and used to predict the future crack lengths with the assumption of linearity in crack propagation. The main failure mechanism of the IGBT device in this paper is the crack propagation in the wire-bond interconnection. The usual aging indicator of such damages is the voltage between the collector and the emitter of current (V_{CE}) that increases with degradation. The analytical model is related to this indicator and it is based on the contact resistance theory and constriction current lines. The proposed model is hence used to build a prognostics model for estimating the remaining useful lifetime (RUL) of IGBT power modules. The prognostics model is illustrated using aging data coming from accelerated power cycling tests with different stress conditions. The first cycling test is under the conditions of stress duration $t_{on} = 3\text{sec}$ and junction temperature swing amplitudes $\Delta T_{j=110}°C$ and the second cycling test is under $t_{on} = 3sec$ and $\Delta T_j = 90°C$. Results show a prognostics capability.

1. INTRODUCTION

The reliability of power electronic devices is important for most power electronic systems. Electronic components, such as IGBTs, assembled in power modules are subjected to high environmental and functional stresses (ambient temperature, vibrations, etc.). All these factors have a strong impact on device reliability and lifetime. From an economic point of view, predictive maintenance may be less detrimental than preventive maintenance performed at fixed time intervals. Consequently, the use of lifetime prognostics tools can be necessary. The problem consists of the health state prediction of power modules in operation to be able to schedule maintenance before the failure of the equipment.

In power electronic systems, two main kinds of models can be built to achieve prognostics: the damage accumulation models and the condition based prediction models. The damage accumulation models can estimate the lifetime of components operating under given usage conditions. The effect of past usage is explicitly modeled by summing up the partial damages. At present, such models, do not specifically represent the physics of degradation to estimate the state of a specific system. An example of this model is the Coffin Manson (Manson, 1966) and Paris's law (Yang, Agyakwa and Johnson, 2013). Research is ongoing to improve these types of models, for example, N. Dornic found a relation between the N_f (number of cycles until failure) with the stress duration t_{on} and junction temperature swing amplitudes ΔT_j (Dornic et al., 2019). The second type, which is condition-based prediction models, is based on the measurement and

extrapolation of a precursor to failure. It assesses the behavior of individual units not only on their usage history but also on expected future load profiles. In other words, it utilizes a degradation model that predicts the future state based on input that describes the current system state and the expected load levels on the system. These component-specific models are generally adaptable and can be developed based on the physics of the system like (Degrenne and Mollov, 2018; Hu et al., 2019) or can be learned from run to failure data using data-driven methods like (Sreenuch et al., 2014; Alghassi, 2016; Liu et al., 2017). T. Sreenuch used the Probabilistic Monte-Carl o method for modeling and online prediction of the remaining useful life (RUL) in an electronic component (Sreenuch et al., 2014). His study was based on the V_{CE} data collected from the electronic component, also Zhen Liu used the Machine learning method to predict RUL for IGBT semiconductors using degradation data (Liu et al., 2017). The model built in this paper as highlighted in the red circle in Fig.1 is classified as a physics-based model in the condition based prediction category.

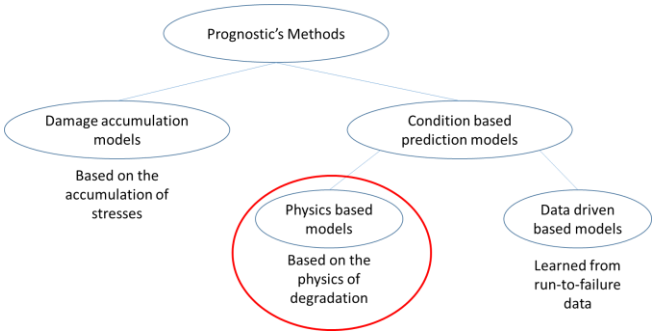

Fig.1: Prognostics models classification.

Based on the previous studies done in this field, this paper presents a new analytical model that describes the degradation in the IGBT module. Then, using this model, a prognostics model is built to predict the RUL.

The remainder of the paper is organized as follows. Section 2 starts by defining different types of degradations that occur in IGBT devices due to aging. Several aging tests were done in SATIE lab that shows the evolution of V_{CE} with the number of cycles. Section 3 presents an analytical model describing the evolution of the dominant degradation that takes place in this module, based on the theory of contact resistance. An online prognostics model is then built-in Section 4 to predict the RUL. The steps for building the model are illustrated. This model is validated by experimental results with different stress conditions. Finally, a conclusion is provided in Section 5.

2. AGING AND DEGRADATION

During the aging of power electronic devices, different types of degradations can take place as shown in Fig.2. The degradation types are: wire-bond degradation that usually leads to heel cracks, wire-bond lift-off due to crack propagation in the wire-bond interconnection with the metallization, top metallization degradation due to grains recrystallization, die-attach degradation that leads to cracks at the die bottom connection, cracks in the metallization ceramic interface, cracks in the ceramic itself, and substrate attach that leads to solder cracks.

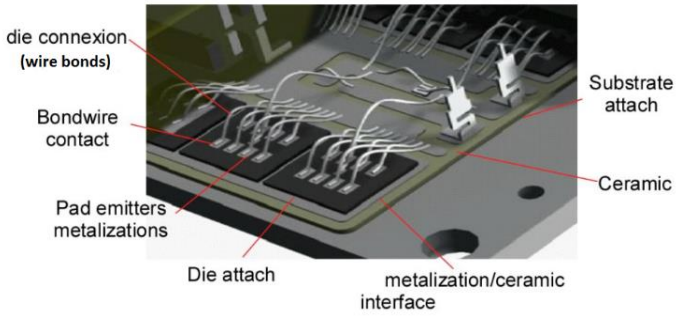

Fig.2: Degradation types in IGBT semiconductors.

In the IGBT module, wire-bond lift-off is a dominant degradation. For this reason, the focus in this paper will be in modeling the crack propagation leading to the lift-off. Fig.3(b). presents crack propagation in the wire-bond interconnection with the metallization pad, and Fig.3(a) presents a lifted wire-bond.

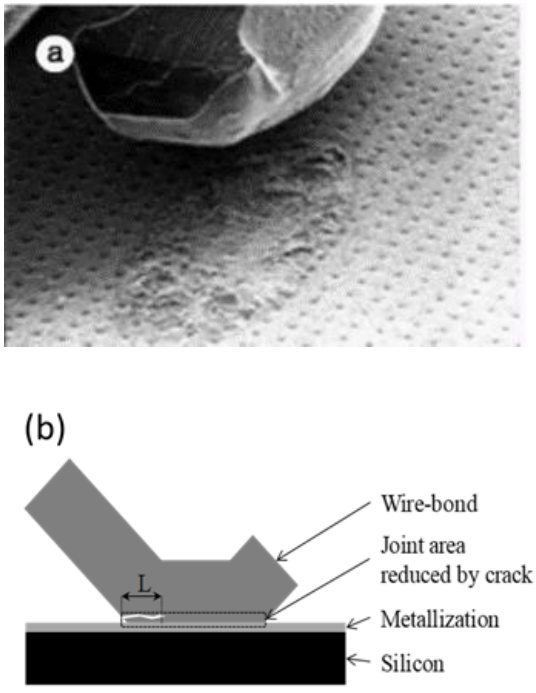

Fig.3: a) wire-bond lift-off (Ciappa, 2002), b) crack propagation in the wire-bond interconnection with the metallization (Degrenne and Mollov, 2018).

Since pure analytical models of damage processes are very complicated to build, failure prediction needs an assist from

experimental data. Thus, it is important to collect information of an aging indicator in the form of a degradation profile that covers failure data that will assist in the prognostics approach.

A way to see the V_{CE} evolution with degradation due to thermal fatigue is obtained by accelerated aging tests like power cycling. This type of test is done in the SATIE Lab. Fig.4 shows experimental data for 4 IGBTs of the same module type until failure. As data from the field are not easy to obtain, these types of accelerated results will be used hereafter for model validation. The dominant degradation observed in these accelerated aging tests was the lift-off due to crack propagation. Hence, we can assume that the voltage variation in the wire-bond contact is the same as the voltage variation between the collector and the emitter.

In Fig.4, the experimental accelerated conditions used are from power pulses with 3sec heating time and 6sec cooling time with power value that leads to 110°C temperature variation.

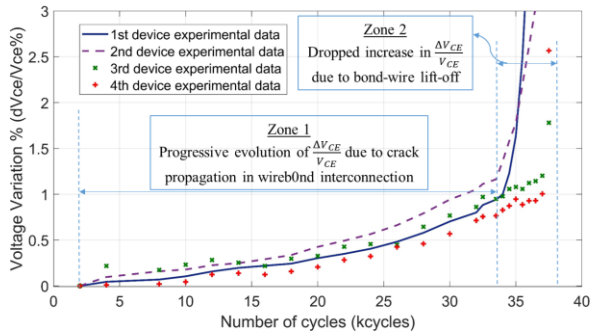

Fig.4: Collector-Emitter voltage variation, and its zones due to types of degradation.

Based on the type of degradation in Fig.4, we divided the lifetime line into 2 zones. Zone 1 is much longer than zone 2; it covers more than 80% of the device's lifetime. It has a progressive evolution in $\Delta V_{CE}/V_{CE}$ due to crack propagation in the wire-bond metallization interconnection, which leads to a decrease in the contact area between wire-bonds and metallization. At the end of this zone, the wire-bonds' lift-off starts. Zone 2 is when the wire-bonds start to lift-off where the failure takes place quickly. The End of Life (EoL) criterion for the failure of these devices is when the $\Delta V_{CE}/V_{CE}$ reaches 5%. Since zone 1 covers more than 80% of the lifetime, and since in zone 2 failure occurs quickly due to lift-off, then it is more important as the first step to model and to predict the degradation in zone 1 than zone 2.

Based on the importance of zone 1, an analytical physics-based model is done to describe the impact of crack propagation on the contact resistance.

3. CONTACT RESISTANCE ANALYTICAL MODEL

In this section, an analytical model is built that estimates the increase of the crack length at the wire-bond contact from the increase in the V_{CE}. This model is then used to predict the RUL, assuming a mean speed linear crack propagation. In comparison to literature, a study done by Degrenne and Mollov (Degrenne and Mollov, 2018) presents a physical model that relates the crack propagation to on-state voltage. Using a specific algorithm, this model is used to predict the RUL with an accuracy of less than ±10%. This model assumes that crack propagation is linear. However, Hu (Hu et al., 2019) built a physical model that relates the crack propagation to the voltage using the Finite Element Method and taking into consideration nonlinear crack propagation. This model took into account also the effects of temperature variation and metallization degradation on the on-state voltage increase.

The model in this paper combines two different models. The first one describes the constriction resistance at the bond contact due to the crack from the wire-bond side. The second one gives the spreading resistance in the metallization due to the current lines flowing from the die, collected by the metallization pad, and going through the bonding wire. The spreading of the current lines is also affected by the crack length. The model is simplified to consider a disc as a surface contact between a cylindrical bond-wire and the metallization as depicted in Fig.5.

Fig.5 presents wire-bond connected to metallization showing the constriction resistance at the contact surface of radius due to the connection between the members and the crack propagation. The constriction resistance is the resistance produced due to the current constricted to pass through the contact area. It can be observed that the equipotential lines start to be not parallel due to current lines constructed in the contact area.

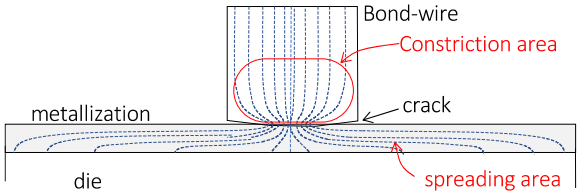

Fig.5: C1 and Model geometry with the constriction and the spreading areas.

Based on Holm's relation (Holm, 1967), the constriction resistance in one member is defined as:

$$R_C = \frac{\rho}{4a} \qquad (1)$$

Equation (1) represents the effect of "ρ" resistivity of the material), and "a" (radius of the contact area), on "R_c" which is the constriction resistance in the wire-bond side. In this

study, we assume the resistivity is constant, which makes the constriction resistance as a function of the radius only.

On the other side, as shown in Fig.6 the resistance of a thin layer (metallization) between $r = a$ and $r = b$ connected to a wire-bond through a contact area of radius "a" as shown in Fig.6 is:

$$R = \frac{\rho}{2\pi t}\left(\frac{b^2}{b^2 - a^2} ln\left(\frac{b}{a}\right) - \frac{1}{2}\right) \qquad (2.1)$$

Equation (2.1) is demonstrated in Appendix A. Where "t" is the thickness of the layer, and "b" is the considered overall radius. In this equation, the parameters "b", "t" and "ρ" are constant. Hence, the resistance of the thin film will be only a function of "a". The constriction resistance of the metallization member under the contact is neglected in comparison with the metallization resistance from $r = a$ to $r = b$.

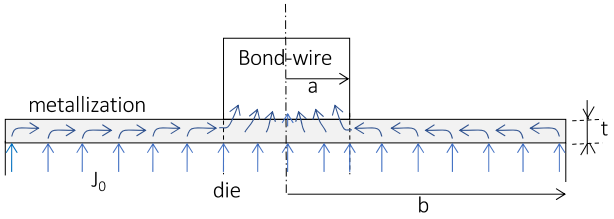

Fig.6: Flow of current from wire-bond to metallization to Die.

Equation (2.1) doesn't include the resistance increase in the metallization due to resistivity increase and/or structure change (recrystallization and grain grooving). Knowing that the resistance of metallization increases with aging due to power cycling as mentioned in (Zhao et al., 2019). Based on that, a factor "w" is multiplied to the resistance of Equation 2.1. No additional measurements were done to fix "w", however, it is assumed to be equal to 2 based on the study of (Zhao et al., 2019) that carries almost the same conditions of power cycling tests used in this study. Other different papers also prove that this value could be increased up to 7 based on the conditions used in the aging tests (Arab et al., 2008).

$$R = \frac{w\rho}{2\pi t}\left(\frac{b^2}{b^2 - a^2} ln\left(\frac{b}{a}\right) - \frac{1}{2}\right) \qquad (2.2)$$

It is necessary to be mentioned that the wire-bond contact shape in IGBT is ellipsoidal. However, Holms book (Holm, 1967) mentioned that for ellipse contact shape the difference can be neglected if the multiplication of the ellipses' major and minor semi-axis is equal to a^2 (which is our situation). Moreover, the dimensions of our metallization are not circular. However, in our study "b" is assessed experimentally. That will give an approximation of the value b, which in any way has a slight effect on the equation's results.

The first model presented by Eq. (1) shows the effect of "a" change on the constriction resistance, and the second model represented by Eq. (2) shows the effect of "a" on the metallization's resistance.

The other values of parameters in Eq. (1) & (2.2) based on the structure are $b = 2\,mm$, radius initial value $a_0 = 332\,\mu m$, $t = 4\mu m$, and $\rho = 3.8 * 10^{-8}\Omega$m.

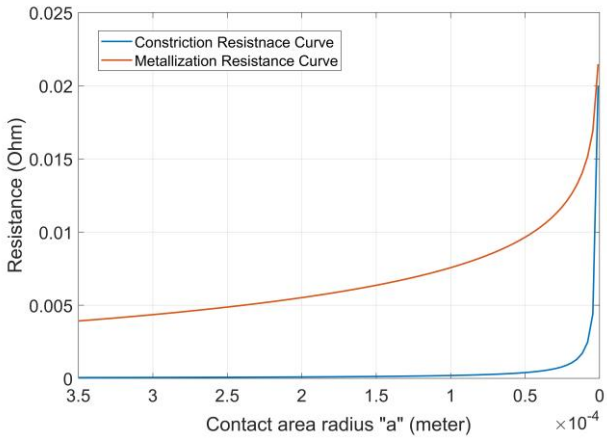

Fig.7: Effect of contact area radius "a" change in Eq. (1) & (2.1) on the resistance.

In Fig.7, the effect of radius changes of the bond contact on both resistances, due to crack propagation, is shown. It is observed that with a decrease in the radius, the two resistances increase. It can be observed that the metallization resistance remains very high compared to that of constriction except when the contact is reduced to a very small radius. The sensitivity of resistance to radius change increases with radius decrease, and it increases in high slope at the last few micrometers.

By adding these two models, we can build a new model that describes the effect of crack propagation (contact area decrease) on the resistance between wire-bond and metallization.

$$R(a) = \frac{\rho}{2}\left(\frac{1}{2a} + \frac{w}{\pi t}\left(\frac{b^2}{b^2 - a^2} ln\left(\frac{b}{a}\right) - \frac{1}{2}\right)\right) \qquad (3)$$

The new model represented by Eq. (3) will be used in the prognostics methodology to predict the remaining voltage variation at each measurement. Besides, as mentioned before, the variation of voltage calculated from Eq. (3) equals the variation of collector-emitter voltage (ΔV_{CE}). The approach is more detailed in the next section.

4. PROGNOSTICS APPROACH

The previous model is then used in the prognostics approach to estimate RUL. Data of four failed IGBTs Fig.4, done by accelerated power cycling test, were used for testing the

prediction. The methodology of prognostics starts with measuring the $\Delta V_{CE}/V_{CE}$ value after a short time of aging to let the degradation take place and the crack propagate. Then, use this value to calculate the contact area radius "a_1" using Eq. (4)-(6). After that, we use the initial contact area radius "a_0" to compute the rate of crack propagation (K_1) using Eq. (7). This rate of crack propagation is used to predict the contact area radius with the assumption of linear crack propagation using Eq. (9).

At first, we have the following equation:

$$\frac{\Delta V_{CE}}{V_{CE,ini}} = \frac{\Delta R(a)_{15W} * I}{V_{CE,ini}} \quad (4.1)$$

"$V_{CE,ini}$" is the initial collector-emitter voltage. "I" is the direct current used. "$\Delta R(a)_{15W}$" is the resistance variation of 15 parallel wire-bonds connected to metallization. Eleven of them are degrading and four are not. This degradation distribution is due to the structural wire bonding in the device used, which leads the current to take less resistive paths. This study is explained in Appendix B.

$$\Delta R(a)_{15W} = R(a_m)_{15W} - R(a_0)_{15W} \quad (4.2)$$

$R(a_0)_{15W}$ represents the resistance of 15 wire-bonds before the degradation start, and $R(a_m)_{15W}$ represents the resistance of the 15 wire-bonds at the m^{th} measurement after degradation took place. Where:

$$R(a_0)_{15W} = \frac{R(a_0)}{15} \quad (5)$$

$$R(a_m)_{15W} = \frac{R(a_m) * R(a_0)}{4R(a_m) + 11R(a_0)} \quad (6)$$

$R(a_0)$ & $R(a_m)$ are calculated using Eq. (3).

After "a_m" is calculated using Equations (4)-(6). we use it to compute "K_m" which is the rate of crack propagation using Eq. (7):

$$K_m = \frac{a_m - a_{m-1}}{n_m - n_{m-1}} \quad (7)$$

Using K_m in Eq. (8), $\overline{K_m}$ is calculated using Eq. (8).

$$\overline{K_m} = \frac{(K_1 + \cdots + K_m)}{m} \quad (8)$$

Where $\overline{K_m}$ is the average crack propagation rate. Using $\overline{K_m}$ in Eq. (9), gives the predicted values of a_n until the crack propagation completes. By compensating the predicted values of a_n in Eq. (4)-(6), we will have the first predicted $\Delta V_{CE}/V_{CE,ini}$'s curve.

$$a_n = \overline{K_m} n + a_0 \quad (9)$$

"n" represents the number of cycles for the prediction process at each measurement m. Which means that at each new measurement "m", a prediction curve that predicts $\Delta V_{CE}/V_{CE,ini}$ is formed. This prediction curve stops when the contact area radius "a_n" reaches zero.

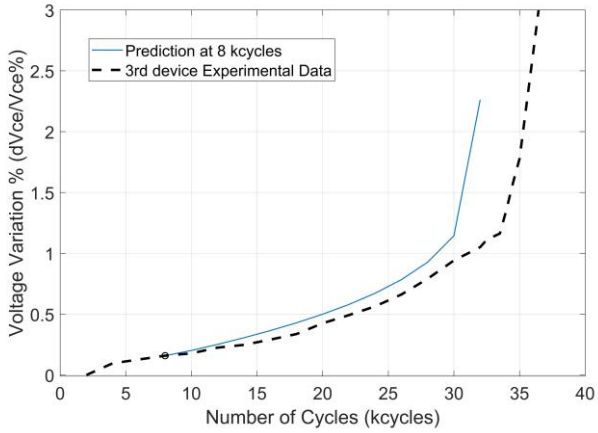

Fig.8: Voltage variation percentage of the first prediction at 8 k.cycles compared to Experimental data.

Table 1. Voltage % measurements with respect to number of cycles. (5 measurements are presented to clarify the process).

	Number of cycle (k.cycles)	$\frac{\Delta V_{CE}}{V_{CE}}$%
First prediction m=1	8	0.16
m=2	12	0.23
m=3	16	0.29
m=4	20	0.43
…	…	…
m=9	34.5	1.58

For instance, for the first prediction at m=1, $\Delta V_{CE}/V_{CE,ini}$ is measured at 8 kilocycles and is equal to 0.16% as shown in Table 1. This value is inserted in Equations (4-6) to calculate the area contact radius a_1. Then, by having a_0 and a_1 in Eq. (7) K_1 is calculated. Then the average rate of crack propagation $\overline{K_1}$ is computed using Eq. (8), which is the same as K_1 for the first prediction.

Then $\overline{K_1}$ is used in Eq. (9) to predict the remaining radiuses until "a" reaches zero. These values of radiuses predicted are then inserted in Equations (4-6) to calculate the predicted $\Delta V_{CE}/V_{CE,ini}$. The first prediction can be observed in Fig.8. After repeating the previous process for several measurements and plotting the predicted $\Delta V_{CE}/V_{CE,ini}$, Fig.9 could be observed. Fig.9 can show the predicted curves for $\Delta V_{CE}/V_{CE,ini}$ at several numbers of cycles. The experimental results in Fig.9 refer to a device aging under $\Delta T = 110°C$ and $t_{on} = 3\ sec$. The experimental data used are filtered with an average moving filter on 3 consecutive points.

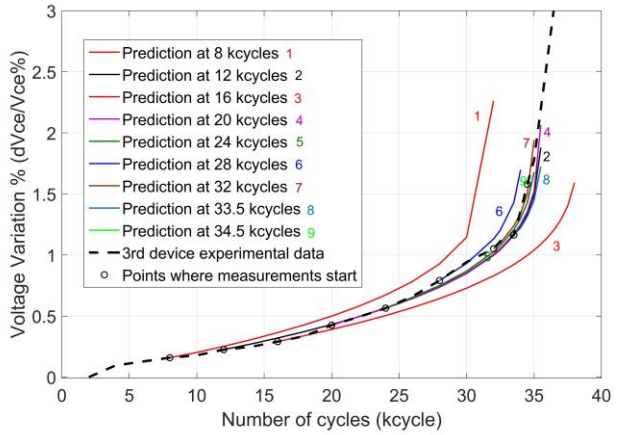

Fig.9: Prediction of the relative increase in V_{CE} for IGBT device under the conditions of $\Delta T = 110°C$ & $t_{on} = 3sec$.

As it can be observed in Fig.9, the prediction was done to estimate the remaining $\Delta V_{CE}/V_{CE,ini}$ curve at each step of measurement. The conventional failure criteria assumption on the collector-emitter voltage indicator is when the $\Delta V_{CE}/V_{CE,ini}$ reaches a 5% increase. However, it is important to note that this threshold is quickly achieved in the last part of aging, which is wire-bond lift-off (zone 2 Fig.4). In Fig.9 the experimental data represented by the dashed black curve is used to validate the predictions. The first and third predictions (8k.cycles, 16k.cycles) are less acceptable than the rest of the curves. This is due to the primary construction of the degradation propagation rate. However, this rate is then tuned after each new measurement due to computing the mean of crack propagation rates, and as you observe for the rest six predictions, the estimated $\Delta V_{CE}/V_{CE,ini}$ is agreeable and can be relied on.

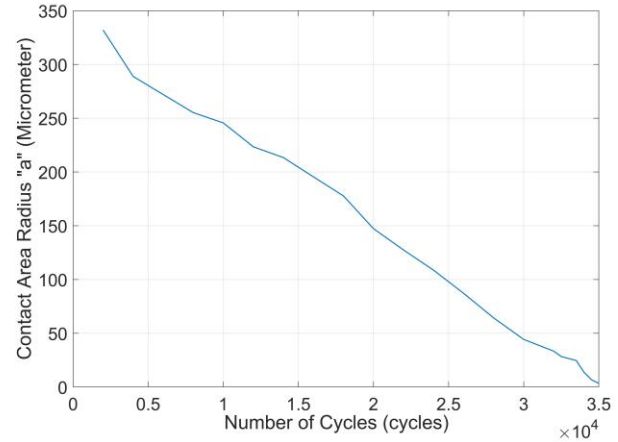

Fig.10: Contact area radius measured (a_m) decrease with the number of cycles for the aging tests done under $\Delta T = 110°C \; and \; t_{on} = 3sec$.

At each mth measurement done a new contact area radius (a_m) is computed. Fig.10 presents the a_m variation with time.

It is shown that the variation of a_m is almost linear with the number of cycles. This verifies the assumption of linear crack propagation with time for the conditions of $\Delta T = 110°C \; and \; t_{on} = 3sec$.

One way to assess the model's robustness is by applying it to different stress conditions. For that, the physical model is also applied to data aged in different conditions.

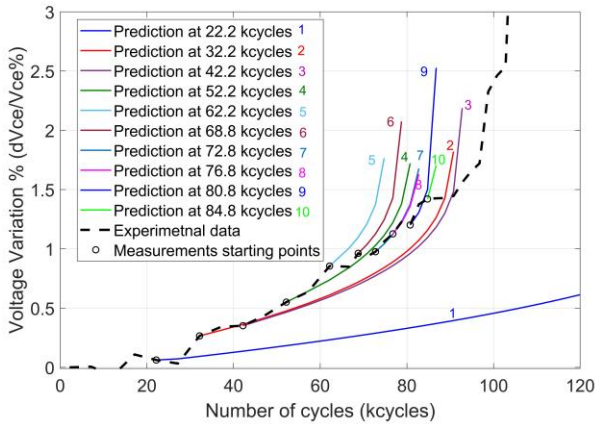

Fig.11: Prediction of the relative increase in V_{CE} for IGBT device under the conditions of $\Delta T = 90°C$ & $t_{on} = 3sec$.

The conditions used in Fig.11 are for an aging test under $\Delta T = 90°C$ and $t_{on} = 3sec$. These tests, as observed, last much more than tests under $\Delta T = 110°C$. The lifetime of the first test is between 35 and 40 k.cycles. However, the lifetime of the next aging test is around 100 k.cycles. This is due to the thermo-mechanical stress effect produced by high temperatures on the degradation. As observed in Fig.11 the first and second curves are far from the experimental curve. This is probably due to an error in experimental data measurement as observed at first 30 k.cycles. After that, the prediction curves start to trend upward as the experimental curve. A percentage of error can be observed in Fig.11. This error, from an industrial point of view, would prevent failures and the corresponding economic losses since the expected predicted failure is before the real failure.

The contact area radius "a_m" decrease related to the last aging test conditions can be observed in Fig.12. The linearity of a_m decrease under $\Delta T = 90°C$ condition is less achieved, especially after the 35 kcycles where before that there exist errors in experimental data measured as shown in the dashed black curve in Fig.11.

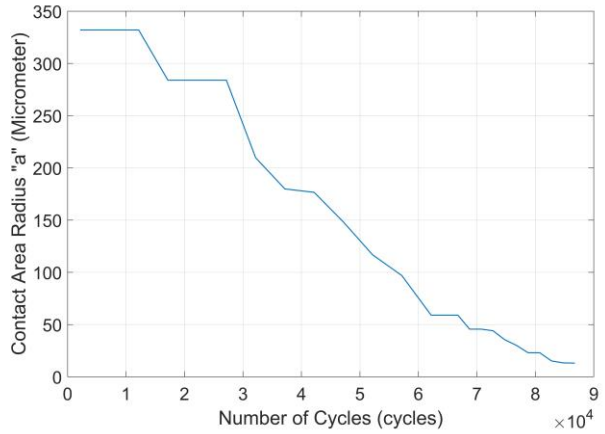

Fig.12: Contact area radius measured (a_m) decrease with the number of cycles for the aging tests done under $\Delta T = 90°C$ and $t_{on} = 3sec$.

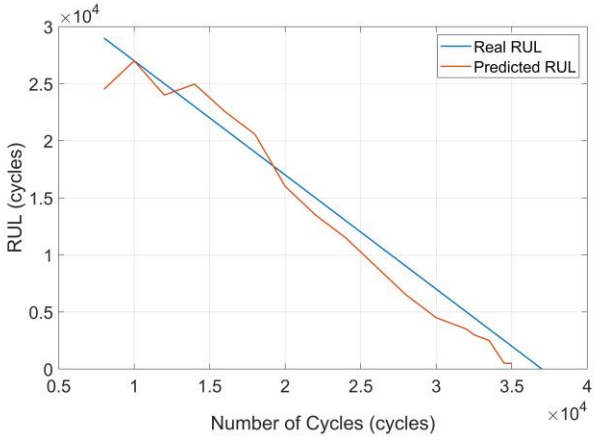

Fig.13: Predict RUL change when applied on aging tests done under$\Delta T = 110°C$ and $t_{on} = 3sec$.

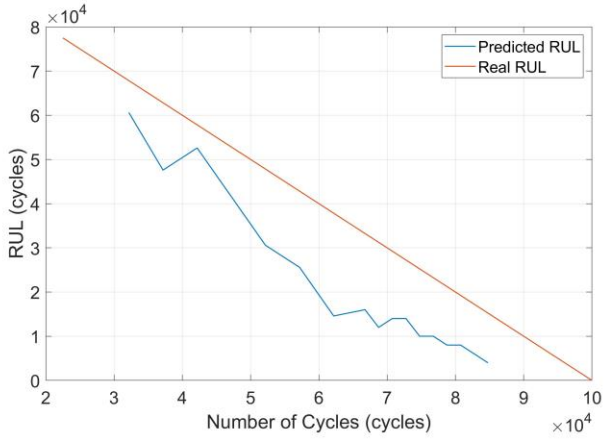

Fig.14: Predict RUL change when applied on aging tests done under$\Delta T = 90°C$ and $t_{on} = 3sec$.

Fig.13 and Fig.14 present the predicted RUL and Real RUL change with the number of cycles for the two different test conditions applied in this study. They start where the first prediction curve took place, except for Fig.14 the curve starts from 32 k.cycles due to the errors observed in the experimental data at the first 30 k.cycles. The values of predicted RULs could be also verified in Fig.9 and Fig.11 where the RUL in this study presents the wire-bond's lift-off. In both figures, the predicted RUL underestimates the failure which could mean that no additional costs the company will pay to failure consequences.

5. CONCLUSION

In this study, a physics-based analytical model is extracted that relates crack propagation to the aging indicator V_{CE}. Since V_{CE} is monitored in real-time operation, then the crack length at each measurement can be calculated. Using the new calculated crack length, the rate of crack propagation is then computed and used to predict the crack lengths until the crack is completed, assuming a linear crack propagation. These predicted crack lengths give the predicted collector-emitter voltage variation using the model built. The predicted V_{CE} identify the end of zone 1, which forms 80% of the total lifetime of the IGBT semiconductor device. It is interesting to be mentioned that the rate of crack propagation is averaged at each new measurement and used for the next prediction. The importance of this work lies under the prediction of the important part of the lifetime in the IGBT. For the evaluation of this prognostics approach, some metrics such as the prognostics horizon and $\alpha - \lambda$ accuracy are evaluated (Saxena, 2008). The proposed model has a good $\alpha - \lambda$ accuracy within 10 % error for the first test condition (ΔT=110°C) while a bad $\alpha - \lambda$ accuracy for the second test condition (ΔT=90°C). The same for the prognostics horizon. This means that this model looses its reliability when changing the aging test conditions. For these reasons, the model should be improved in further studies. One should think about developing a hybrid model by combining the proposed one with a data-driven model.

REFERENCES

Alghassi, A. (2016) Prognostics and Health Management of Power Electronics. CRANFIELD UNIVERSITY.

Arab, M. et al. (2008) 'Experimental investigations of trench field stop IGBT under repetitive short-circuits operations', PESC Record - IEEE Annual Power Electronics Specialists Conference, (1), pp. 4355–4360. doi: 10.1109/PESC.2008.4592645.

Ciappa, M. (2002) 'Selected failure mechanisms of modern power modules', Microelectronics Reliability, 42(4–5), pp. 653–667. doi: 10.1016/S0026-2714(02)00042-2.

Degrenne, N. and Mollov, S. (2018) 'Diagnostics and Prognostics of Wire-Bonded Power Semi-Conductor Modules subject to DC Power Cycling with Physically-

Inspired Models and Particle Filter', Phme 2018, pp. 1–10.

Dornic, N. et al. (2019) 'Stress-Based Model for Lifetime Estimation of Bond Wire Contacts Using Power Cycling Tests and Finite-Element Modeling', IEEE Journal of Emerging and Selected Topics in Power Electronics, 7(3), pp. 1659–1667. doi: 10.1109/JESTPE.2019.2918941.

Holm, R. (1967) Electric Contacts. Berlin, Heidelberg: Springer Berlin Heidelberg. doi: 10.1007/978-3-662-06688-1.

Hu, K. et al. (2019) 'Cost-Effective Prognostics of IGBT Bond Wires with Consideration of Temperature Swing', IEEE Transactions on Power Electronics, (December), pp. 1–1. doi: 10.1109/tpel.2019.2959953.

Liu, Z. et al. (2017) 'Remaining useful life estimation of insulated gate biploar transistors (IGBTS) based on a novel volterra K-nearest neighbor optimally pruned extreme learning machine (VKOPP) model using degradation data', Sensors (Switzerland), 17(11). doi: 10.3390/s17112524.

Manson, S. S. (1966) thermal stress low-cycle fatigue. New York: McGraw-Hill.

Sreenuch, T. et al. (2014) 'Probabilistic Monte-Carlo Method for Modelling and Prediction of Electronics Component Life', International Journal of Advanced Computer Science and Applications, 5(1), pp. 96–104. doi: 10.14569/ijacsa.2014.050113.

Yang, L., Agyakwa, P. A. and Johnson, C. M. (2013) 'Physics-of-failure lifetime prediction models for wire bond interconnects in power electronic modules', IEEE Transactions on Device and Materials Reliability. IEEE, 13(1), pp. 9–17. doi: 10.1109/TDMR.2012.2235836.

Zhao, J. et al. (2019) 'A study on the effect of microstructure evolution of the aluminum metallization layer on its electrical performance during power cycling', IEEE Transactions on Power Electronics. IEEE, 34(11), pp. 11036–11045. doi: 10.1109/TPEL.2019.2895695.

Saxena, A., Celaya, J., Balaban, E., Goebel, K., Saha, B., Saha, S., & Schwabacher, M. (2008, October). Metrics for evaluating performance of prognostic techniques. In 2008 International Conference on Prognostics and Health Management (pp. 1-17). IEEE.

BIOGRAPHIES

Mohamad Nazar received the Dipl. Eng. in aerospace engineering from KNT University of Technology, Tehran, Iran in 2018. The final project was on computing aerodynamic coefficients for a flight vehicle. Then he received his M.Sc. in Electrical Engineering from Paris-Saclay University, Paris, France in 2019. He passed an internship in the Laboratory of New Technology, French National Institute for Transport and Safety Research (IFSTTAR), Versailles, France, working on modeling the degradation in power module devices for prognostics purposes. Now he is doing his Ph.D. in Mitsubishi Electric Research and Development Center Europe (MERCE) and IFSTTAR lab working on Prognostics and Health Management (PHM) approaches in IGBT power modules to predict the remaining useful lifetime (RUL).

Ali Ibrahim received the Dipl. Eng. degree in electrical and electronics from Lebanese University, Beirut, Lebanon, in 2000, the M.Sc. degree in the signal, image, speech, and telecommunications from the National Polytechnic Institute of Grenoble, France, in 2002, and the Ph.D. degree in signal processing from the Jean Monnet University, Saint-Etienne, France, in 2008. He is currently a member of a research team on "Reliability testing of power electronic devices" of the SATIE laboratory – Gustave Eiffel University. He is involved in different collaborative research programs and his research interests include lifetime prediction and reliability of power electronic semiconductors.

Zoubir Khatir received the Dipl. Ing. degree in solid-state physics and the Ph.D. degree from the Institute National des Sciences Appliqués de Toulouse, Toulouse, France, in 1984 and 1988, respectively. He has been with the Laboratory of New Technology, French National Institute for Transport and Safety Research, Versailles, France, since 1988, where he was in charge of high-power semiconductor device modeling and computer-aided design tool development. He is currently a Senior Scientist with the SATIE Laboratory, French Institute of Science and Technology for Transport, Development and Networks, Versailles, France. His current research interests include the reliability in high-temperature environments of silicon and wide bandgap high-power electronic devices in the field of transport applications.

Nicolas Degrenne received M.Sc. and Ph.D. degrees in the field of Electrical Engineering from the "Institute National des Sciences appliqués" and from "Ecole Centrale" Lyon, France, in 2008 and 2012, respectively. He joined Mitsubishi Electric R&D Centre Europe, Rennes, France as a researcher in 2013 and as a research manager in 2019. His fields of interest are the Integration, Reliability, Robustness, Diagnostics and Prognostics of Power Electronic Systems.

Zeina Al Masry received her Ph.D. in Applied Mathematics from the University of Pau and Pays de l'Adour in France in 2016. Since 2017, she joined ENSMM (Ecole Nationale Supérieure de Mécanique et des Microtechniques) in Besançon France as an Associate Professor. She is doing her research activities at the FEMTO-ST institute in the Prognostics and Health Management (PHM) research group. Her research works concern stochastic processes and applied statistics for PHM applications.

APPENDIX A

J_0 is the vertical current density in the die. I_1 is the total current from Die under the contact where $I_1 = J_0\pi a^2$. I_2 is the total current from the Die outside the contact where $I_2 = J_0\pi(b^2 - a^2)$, and $I = I_1 + I_2$.

Based on the current law:

$$i(r) - i(r + dr) = J_0 2\pi r dr \tag{10}$$

"$i(r)$" is the current going out from the cell laterally and it is at distance r from the center of the metallization as shown in Fig. 12. "$i(r + dr)$" is the current flowing inside the cell laterally and it is at a distance $r + dr$. And $J_0 2\pi r dr$ represents the current flowing upward from the die to the metallization going inside the cell.

Equation (10) is integrated from "r" to "b" knowing that $i(b) = 0$. The following equation will be formulated:

$$i(r) = -\pi J_0(b^2 - r^2) \tag{11}$$

Where $i(r)$ is the lateral current in the metallization.

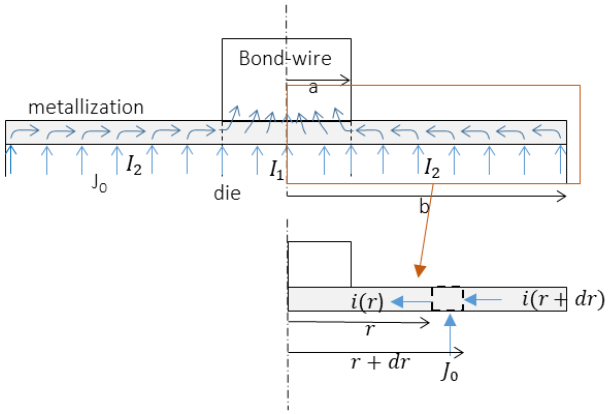

Fig.12: current distribution from metallization to Die and a zoomed part facilitates the understanding of current integration.

Let $J(r)$ be the lateral current density in the metallization at r.

$$J(r) = \frac{i(r)}{2\pi r t} = \sigma E(r) \tag{12}$$

where E is the electric field in the radial direction and σ is the electrical conductivity of the material. By compensating $E = -dV/dr$ and Eq.(11) in Eq.(12) the following equation is formed for voltage variation with r:

$$dV = \frac{\rho J_0}{2t}\frac{b^2 - r^2}{r}dr \tag{13}$$

Then, Eq. (13) is integrated from "a" to "b" knowing that voltage at b is $V(b) = 0$ to have the following voltage equation:

$$V(a) = \frac{-\rho J_0}{2t}\left(b^2 ln\frac{b}{a} - \frac{1}{2}(b^2 - a^2)\right) \tag{14}$$

The equivalent resistance of metallization seen between $r = a$ and $r = b$, can be written as:

$$R_{\text{met.}} = \frac{(\text{V(b)} - \text{V(a)})}{\text{I}_2} \tag{15}$$

Then

$$R_{met.} = \frac{\rho}{2\pi t}\left(\frac{b^2}{b^2 - a^2} ln\frac{b}{a} - \frac{1}{2}\right) \tag{16}$$

APPENDIX B

It is mentioned in the Prognostics Approach section that 11 wire-bonds are degrading and 4 are not degrading assuming that the 11 wire-bonds have the same rate of degradation. Fig.13 presents a top view image for the IGBT device, where it is shown the wire-bonds distribution on the metallization of IGBT (red rectangles) and of the diode (yellow rectangle). You can observe that the wire-bond distribution on the IGBT is divided into two zones. Zone 1 contains 6 wire-bonds connected to the metallization, while zone 2 contains 9 wire-bonds connected to the metallization, knowing that zone 1 is wider than zone 2. This motivates and allures us to study the current distribution in the different wire-bonds after being collected in the metallization.

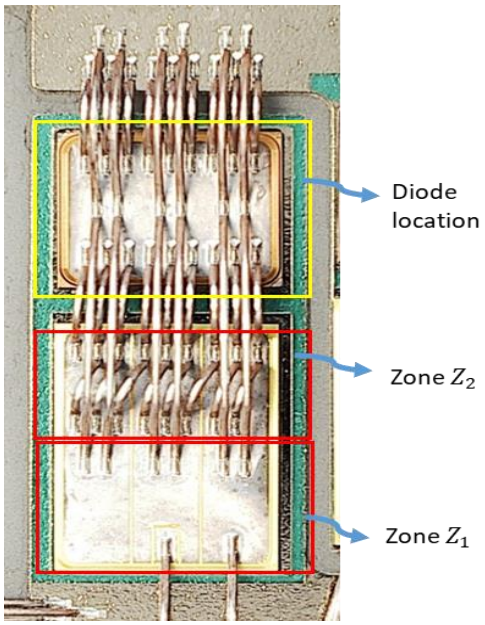

Fig.13: Top image for the IGBT and the diode showing the metallization and wire-bonds distribution on it.

For a deeper discussion, Fig.14 is introduced to facilitate understanding of the current distribution in the wire-bonds. Fig.14 shows the current vertically directing upward to be collected in the metallization (black colored). This metallization is very thin ($\simeq 4\,\mu m$) compared to the wire-bond radius ($\simeq 350\mu m$) which will make the current highly prefer to pass through wire-bonds than the metallization, letting themselves pass through less distance of metallization as possible. Based on this theory, the current collected in metallization in part "d" will continue to pass through the 6 wire-bonds of zone Z_1, avoiding the metallization path of part "c". The percentage of current collected in part "d" is 45% of the whole current and this is due to the 45% area of the whole metallization assuming that the current is uniformly collected in the metallization. In part "c", the current will also continue to pass through the 6 wire-bonds of zone Z_1, and this is due to the less resistive path. Since, if the current of part c passes through the 9 wire-bonds, they are forced to pass also through the metallization of part "a", which is a high resistive path. The percentage of current collected in part "c" is 11%. Finally, in part "b" the current will continue to pass through the 9 wire-bonds of zone Z_2, avoiding passing through extra metallization path in part "c". Metallization in part "b" collects 44% of the whole current.

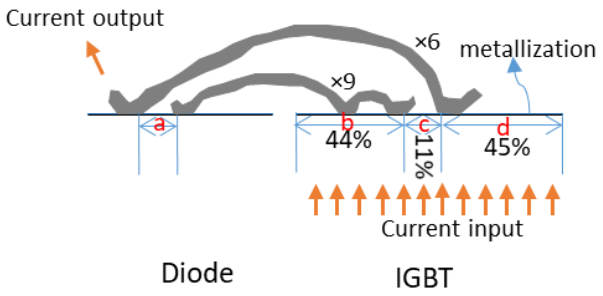

Fig.14: Schematic side view for the IGBT that helps in understanding the current distribution in the different wire-bonds.

Based on the previous study, 56% of the current will pass through the 6 wire-bonds and 44% will pass through the 9 wire-bonds.

Let I_S be the current in each of the 9 wire-bonds of zone Z_2, and I_B the current in each of the 6 wire-bonds of zone Z_1 assuming that the current is uniformly distributed in each zone based on the symmetrical wire bonding on the metallization. Then we have:

$$I_B = \frac{0.56}{6} I = 0.0933I \tag{17}$$

The same for I_S:

$$I_S = \frac{0.44}{9} I = 0.0488I \tag{18}$$

Where I is the total current. By compensating the total current of Eq. (17) in the total current of Eq. (18), the following equations are formed:

$$I_S = 0.524 I_B \Rightarrow \; 9I_S = 4.71 I_B \simeq 5 I_B \tag{19}$$

Equation (19) means that the current passing in the 9 wire-bonds of zone Z_2 can be distributed in 5 wire-bonds to have in each one of these 5 the same current density as the 6 wire-bonds in zone Z_1. This gives the ability to assume that the current I_S is passing through 5 wire-bonds. Thus, it can be also assumed that the crack is just in these 5 wire-bonds. It is also assumed that the crack propagation in the 11 degrading wire-bond is the same.